LAWRENCE
LIVERMORE
NATIONAL
LABORATORY

LLNL-JRNL-766084

# Stability and metallization of solid oxygen under high pressure

S. F. Elatresh, V. Askarpour, S. A. Bonev

January 17, 2019

Physical Chemistry Chemical Physics

## Disclaimer

This document was prepared as an account of work sponsored by an agency of the United States government. Neither the United States government nor Lawrence Livermore National Security, LLC, nor any of their employees makes any warranty, expressed or implied, or assumes any legal liability or responsibility for the accuracy, completeness, or usefulness of any information, apparatus, product, or process disclosed, or represents that its use would not infringe privately owned rights. Reference herein to any specific commercial product, process, or service by trade name, trademark, manufacturer, or otherwise does not necessarily constitute or imply its endorsement, recommendation, or favoring by the United States government or Lawrence Livermore National Security, LLC. The views and opinions of authors expressed herein do not necessarily state or reflect those of the United States government or Lawrence Livermore National Security, LLC, and shall not be used for advertising or product endorsement purposes.

ARTICLE TYPE

Cite this: DOI: 00.0000/xxxxxxxxxx

# Stability and metallization of solid oxygen at high pressure

Sabri F. Elatresh[a,b] and Stanimir A. Bonev*[c]

Received Date
Accepted Date

DOI: 00.0000/xxxxxxxxxx

**The phase diagram of oxygen is investigated for pressures from 50 to 130 GPa and temperatures up to 1200 K using first-principles theory. A metallic molecular structure with the $P6_3/mmc$ symmetry ($\eta'$ phase) is determined to be thermodynamically stable in this pressure range at elevated temperatures above the $\varepsilon(O_8)$ phase. Crucial for obtaining this result is the inclusion of anharmonic lattice dynamics effects and accurate calculations of exchange interactions in the presence of thermal disorder. We present analysis of electronic, structural, and thermodynamic properties of solid oxygen at 0 K and finite temperature with hybrid exchange functionals, including a comparison with available experimental data.**

Oxygen has received a great deal of attention because it is a fundamental element, one of the most abundant on earth and the only one known with a diatomic molecule that carries a magnetic moment. It has a rich high pressure ($P$) phase diagram with multiple solid phases exhibiting diverse physical properties[1–16]. One of the most interesting structures among them is the $\varepsilon$-phase, which is stable over a large pressure range. It has been studied extensively both theoretically[17–26] and experimentally by X-ray diffraction[2,27–29] and spectroscopic measurements [30–34].

Despite theoretical works suggesting that $\varepsilon$ phase has $C2/m$ symmetry [2,27,28,35] and its strong infrared absorption[3] alluding to $O_2$ molecules forming larger units[18,31], it took considerable experimental effort to define the exact structure as $\varepsilon(O_8)$ or $\varepsilon((O_2)_4)$ clusters[4,36,37]. Upon compression to 96 GPa, $\varepsilon(O_8)$ transforms to the metallic $\zeta$ phase[2,12], which is superconducting at 0.6 K [13]. Experimentally, Goncharov et al. [38] proposed an $\eta'$ phase in the pressure range of 44 to 90 GPa and at temperatures ($T$) near 1000 K. It was suggested to be an isostructure of the $\eta$-O phase previously proposed at low pressures[7,39,40].

Most previous theoretical studies have been limited to 0 K. The initial theoretical works[41] suggested $C2/m$ as the best candidate for $\zeta$-$O_2$ but exhibited significant disagreements between the calculated and measured $\varepsilon$-$\zeta$ transition pressures, as well as the structures of the $\varepsilon$ and $\zeta$ phases. Subsequent studies[20–26] showed that the use of density functional theory (DFT) at the level of the generalized gradient approximation (GGA) leads to incorrect structural and energetic predictions for the high pressure $\varepsilon$ and $\zeta$ phases. Moreover, these works demonstrated that hybrid-type exchange[20,21,23–26] and meta GGA with van der Waals[22] functionals can predict correctly the $\varepsilon$-$\zeta$ transition pressure, as well as lattice parameters and vibrational spectra as a function of pressure.

Here we report results on the phase diagram of solid oxygen for pressure up to 130 GPa, at both 0 K and finite $T$. First, we establish the accuracy of the hybrid exchange functional employed in this study by computing the structural and energetic properties of the known oxygen structures, $\varepsilon$ and $\zeta$, as a function of pressure at 0 K. Next, we focus on elevated temperatures where we show that inclusion of anharmonic effects and accurate exchange energy calculations in the presence of thermal disorder are both crucial for determining the stability of $O_2$ phases.

## Results and Discussion

### Low Temperature Stability

We start by examining oxygen at 0 K in the pressure range of up to 130 GPa and consider the relevant structures: $\eta'$ [38], $\varepsilon$ ($O_8$) [4], and $\zeta$ ($C2/m$) [41] (e.g. see Supplementary Information (SI) Fig. S1). It is well known that the GGA introduces errors in the ground state energy calculations, which depend on the electronic properties of the system; the overall tendency is to favor better metals. Because there are notable differences among the electronic properties of the competing structures– $\varepsilon(O_8)$ is an insulator while $\zeta(C2/m)$ and $\eta'$ are metallic (Fig.'s S2 and S3), there are non-cancellation

[a] Department of Physics, University of Guelph, Guelph, Ontario, Canada N1G 2W1
[b] Department of Chemistry and Chemical Biology, Cornell University, Baker Laboratory, Ithaca, NY 14853-1301, USA.
[c] Lawrence Livermore National Laboratory, Livermore, California 94550, USA.
*E-mail: bonev@llnl.gov

† Electronic Supplementary Information (ESI) available: See DOI: 00.0000/00000000.

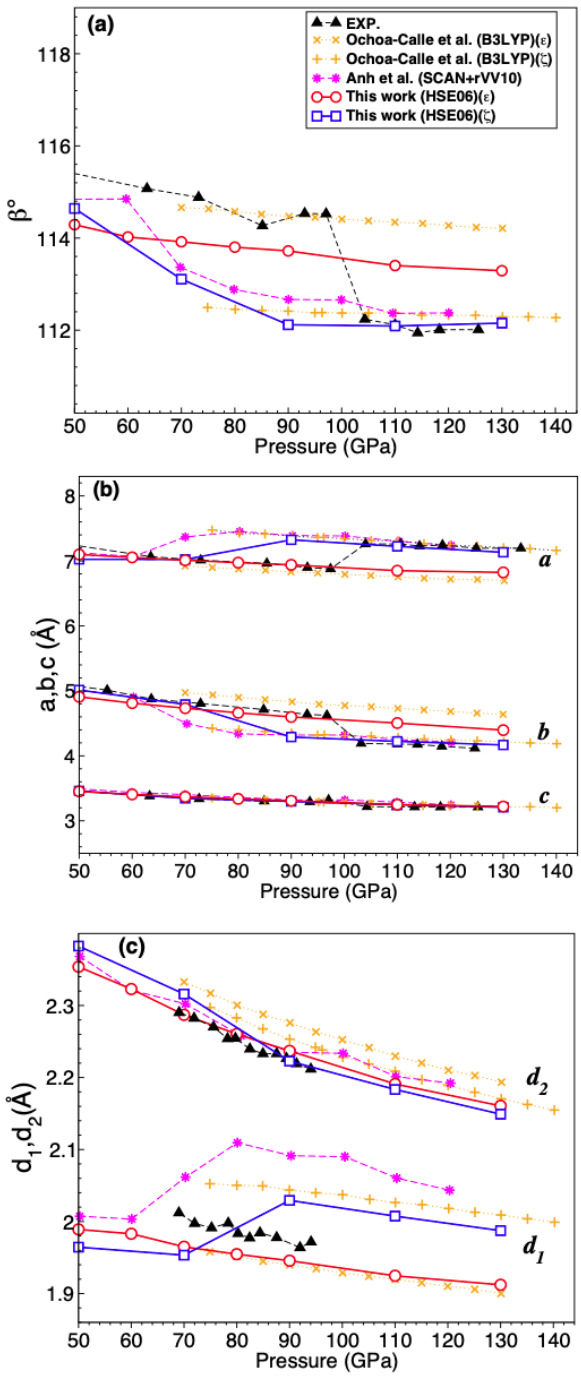


**Fig. 1** (Color online) Optimized structural parameters of the $\varepsilon$ and $\zeta$ crystal structures of oxygen with $C2/m$ symmetry. Here $\beta$ is the monoclinic angle, $a$, $b$, $c$ the lattice parameters of the conventional unit cell, and $d_1$ and $d_2$ (see SI Fig. S4 for graphical illustration of the structure) . The legend in (a) refers to panels (b) and (c) as well. The results from this work are compared to previous theoretical results by Anh et al.[23] and Ochoa-Calle et al.[22], and to experimental data from (a) and (b) Weck et al.[28] and (c) Fujihisa Fujihisha et al.[36]. Note the the experimental data for $d_1$ and $d_2$ is only in the pressure range of stability of $\varepsilon$.

of GGA errors leading to significant underestimation of the metallization pressure of oxygen computed within this approximation. This fact was pointed out by Elatresh et al[20,21] where the Heyd-Scuseria-Ernzerhof (HSE06) approximation [42] was used to correct the GGA energies. Comprehensive studies of various hybrid-type exchange functionals were carried by Ochoa-Calle et al.[23–26] and with meta GGA (SCAN)+van der Waals (rVV10) by Anh et al.[22] who showed that these methods yield satisfactory results for a number of experimental properties.

To validate the accuracy to the HSE06 approximation used in this study, we first compare the structural properties of oxygen computed with HSE06 to the best results from Ochoa-Calle et al.[23,24] and Anh et al.[22], and to available experimental data[36]. The parameters for the $\varepsilon$ ($O_8$) and$\zeta$ ($C2/m$) structures are shown in Fig. 1 as a function of pressure. Further details, including equation of state, data for $\eta'$, and comparison to GGA are provided in Supplementary Information (Fig. S5). Note that $\varepsilon(O_8)$ has the same space group symmetry as the $\zeta$ phase, namely, $C2/m$, and with atoms occupying identical Wyckoff positions in the two structures: 2(i), 2(i) and 4(j). Within HSE06, the lattice parameters of $\zeta(C2/m)$ evolve towards that of $\varepsilon(O_8)$ as pressure decreases, and the two structures become identical below 50 GPa (Fig. S6).

As evident from Fig. 1, the HSE06 leads to excellent agreement with the experimental data, which is at least as good as that of the B3LYP and SCAN+rVV10 functionals. Notice that HSE06 has the best agreement with the experimental data for the $d_1$ and $d_2$ intermolecular distances (Fig. 1 (c)). Its worst result is for the monoclinic angle $\beta$ of $\varepsilon$, which it only underestimates by less than one degree. The excellent performance of HSE06 is consistent with our previous studies of phase transitions under high pressure[43,44].

The relative enthalpies of $\varepsilon(O_8)$, $\zeta(C2/m)$ and $\eta'$ computed wtih the GGA and HSE06 functionals are shown in Fig. 2. Notice that $\varepsilon(O_8)$ is most strongly affected by the HSE06 corrections to GGA. At around 90 GPa, it is lowered by as much as 53 and

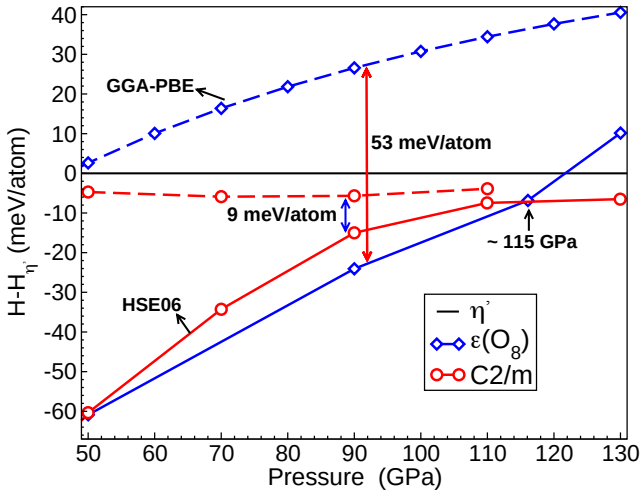


**Fig. 2** (Color online) Enthalpies of $\varepsilon(O_8)$ and $\zeta(C2/m)$ relative to $\eta'$ oxygen. Dashed and solid lines are GGA-PBE and HSE06 calculations, respectively. Within HSE06, $\varepsilon(O_8)$ is stable from 50 to 115 GPa, which consistent with the measurement [4]. As explained in the text, within HSE06, $\varepsilon(O_8)$ and $\zeta(C2/m)$ converge to the same structure below 50 GPa.

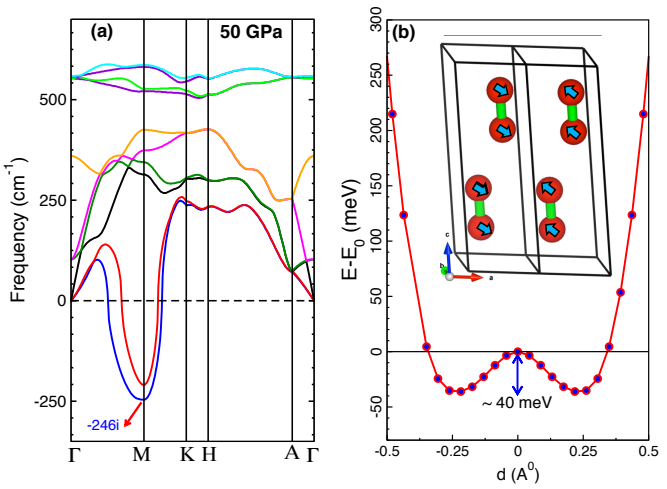


**Fig. 3** (a) Phonon spectra of $\eta'$ oxygen at 50 GPa computed within the harmonic approximation as explained in the text. (b) Change in energy as a function of atomic displacement, $d$, from the equilibrium positions for the unstable transverse acoustic mode at M. The arrows indicate the atomic displacements for the corresponding phonon eigenvector.

44 meV/atom relative to $\eta'$ and $\zeta(C2/m)$, respectively. These corrections are sufficient to make $\varepsilon(O_8)$ the preferred structure in the $P$-$T$ region where it has been observed experimentally. The larger effect of hybrid exchange on $\varepsilon(O_8)$ is understood by the fact that (at 0 K) this phase is insulating for $P < 107$ GPa, where upon further compression it metallizes by way of band overlap. The computed closure of the band-gap at 107 GPa and 0 K (Fig. S3(D)) is in a good agreement with experimental observations [2,12] for oxygen remaining non-metallic until 96 GPa pressure. Our analysis (see SI Fig.'s S7 and S8) indicates that in order to reproduce this metallization pressure, it is necessary to perform both structural optimization and electronic band structure calculations using hybrid exchange.

To summarize, we have shown that the HSE06 functional describes accurately the structural and energetic properties of solid oxygen at low temperature in the ~50–100 GPa range, in agreement with the available experimental data and previous beyond-GGA calculations.

### Stability at Elevated Temperatures

Our analysis for the thermodynamic stability of $O_2$ at elevated $T$ starts with examining the phonon dispersions of the $\eta'$ and $\varepsilon$-$O_8$ phases at 50 GPa. For the $\eta'$ phase, converged dynamical matrices yield imaginary phonon frequencies (see Fig. 3(a)). This could mean that the structure is mechanically unstable and is probably the reason why it was not found in previous structure search studies. However, depending on the nature of the soft phonon modes, it can be stabilized at finite $T$, or even at 0 K due to quantum zero point motion. Hence, we have examined more closely the phonon modes where the instability is most pronounced using the frozen phonon method. The results in Fig. 3(b) show that the unstable mode is indeed a shallow double well potential. The appearance of a double well potential associated with a structural instability is similar to what has been observed in other elements such as Ca [45]. However, compared to Ca, the potential barrier in $\eta'$-$O_2$ is much higher. Nevertheless, this mode can be thermally stabilized at $T$ of around several hundred K and is likely to contribute significantly to the entropy of the $\eta'$ phase at elevated $T$. For determining the thermodynamic stability of $\eta'$-$O_2$, it is therefore necessary to go beyond the quasi-harmonic approximation. Its Gibbs free energies ($G$) at finite $T$ were computed using first principle molecular dynamics (FPMD) simulations in the ~49–70 GPa $P$ range and $T = 500$, 800 and 1200 K, which captures most of the anharmonic free energy. For $\varepsilon(O_8)$, where the harmonic approximation is sufficient, vibration density of states (VDOS) and phonon free energy terms were calculated from DFPT.

A comparison of the VDOS of the $\eta'$ and $\varepsilon(O_8)$ phases is shown in Fig. 4(a), from which the anharmonicity of the former is evident. The enthalpies of the two phases as a function of $T$ are shown in Fig. 4(b). Within GGA, the enthalpy of $\eta'$ remains lower in the entire temperature range of interest. The lower frequency modes of $\eta'$-$O_2$ slightly lower its enthalpy relative to that of $\varepsilon(O_8)$, but the effect is small and after adding the HSE06 correction computed earlier, the enthalpy of $\varepsilon(O_8)$ becomes lower at all temperatures. The soft modes have much more pronounced effect on the entropy ($S$). The $TS$ terms are plotted as a function of temperature in Fig. 4(c). As expected, the $\eta'$ phase has higher entropy. At 750 K, its $TS$ is 37 meV/atom higher than that of the $\varepsilon(O_8)$ phase. In the context of relative stabilities of molecular crystals, this is a relatively large value. However, it is still not sufficient to overcome the enthalpy differences between the two phases and to make $\eta'$ preferred at elevated temperatures.

In order to find a clue that may solve the problem for the finite temperature stability, we examine the local structural oder

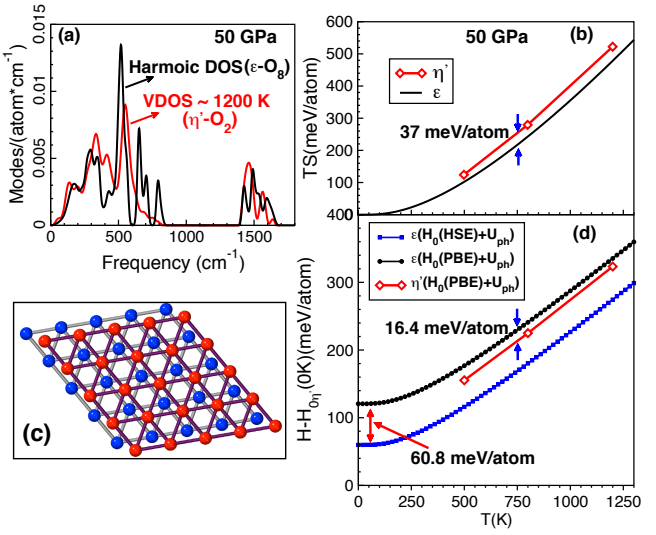


**Fig. 4** (Color online): (a) Vibration density of states (VDOS); (b) $TS$ (temperature times entropy); and (d) enthalpies for the $\eta'$ (red) and $\varepsilon(O_8)$ (black) phases relative to the 0 K $\eta'$ structure enthalpy. The relative enthalpies are shown with and without HSE06 corrections. (c) View of the $\eta'$ phase along the c-axis (bond direction).

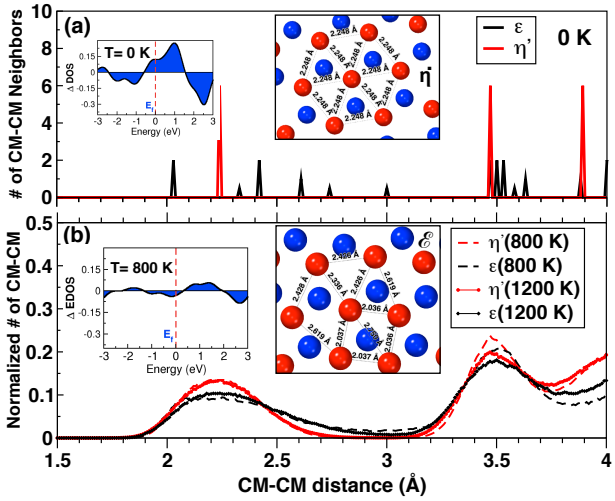


**Fig. 5** (Color online) Comparison of CM-CM distance distributions of the $\varepsilon(O_8)$ (black) and $\eta'$-$O_2$ (red) structures at 50 GPa and (a) 0 K and (b) high temperature. The insets on the right side show the equilibrium atomic positions of $\eta'$ (in (a)) and $\varepsilon(O_8)$ (in (b)). The insets on the left side show the differences in the electronic density of states (EDOS) of the two structures near the Fermi level at 0 and 800 K. The difference is much diminished at the higher temperature.

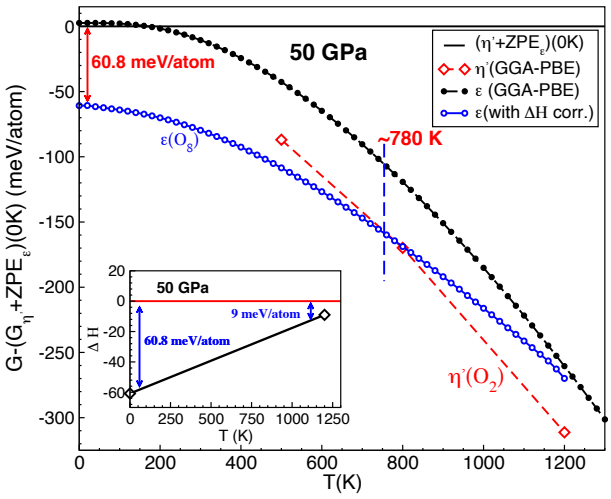


**Fig. 6** (Color online) Gibbs free energies of $\varepsilon(O_8)$ and $\eta'$-$O_2$ at 50 GPa as a function of temperature, relative to the 0 K result for $\eta'$. For comparison, relative energies are computed within both GGA and HSE06. The inset shows the HSE06 corrections to the relative $\varepsilon(O_8)$-$\eta'$ enthalpies. Note that we have added the zero point energy (ZPE) of $\varepsilon(O_8)$ to the reference energy in order to have 0 K transitions consistent with the Fig. 2 plot; this does not affect the finite-$T$ transitions.

of the $\varepsilon(O_8)$ and $\eta'$ phases. The atomic arrangements in the two structures are shown in the insets of Fig. 5. In both cases, the molecules are arranged in layers, with their bonds perpendicular to the the layers. Fig. 5(a) shows a distribution of distances between the molecular center of masses (CM) of the 0 K crystals. The CM-CM distributions look quite different and it is clear that $\eta'$ is the more symmetric structure (Fig. S9). However, if we examine the atomic arrangements shown in the insets of Fig. 5, we see that locally the $\varepsilon(O_8)$ phase can be viewed as a distortion of the hexagonal molecular arrangements found in the $\eta'$ phase. This observation suggests that the introduction of thermal disorder may bring the average local order of the two structures closer to each other. CM-CM distance distributions computed from finite-temperature FPMD trajectories (Fig. 5(b)) show that this is indeed the case. Namely, the short range orders of the two structures become similar, on average, in the presence of thermal disorder. As seen in the insets in Fig. 5 and Fig.'s S10 & S11, the difference of the electronic density of states between the two structures near the Fermi energy also diminish with temperature.

The implication of the above observations is that the hybrid exchange corrections to the energies computed on ideal 0 K crystals may not be adequate at fine $T$. Indeed, exchange interactions are in principle short-range. In the HSE06 implementation here, the effective range of the Hartree-Fock exchange is around 4 A (hence the 4 A CM-CM range shown in Fig. 5). Therefore, if the local orders of the two structures become similar at elevated $T$, then the differences between their HSE06 corrections are also expected to diminish with temperature. This, in turn, will make $\eta'$-$O_2$ more competitive at finite $T$ compared to the 0 K case.

We have therefore performed HSE06 calculations on atomic configurations taken from the FPMD trajectories at 1200 K. The results reveal that at 50 GPa and 1200 K the hybrid exchange correction of $\eta'$-$O_2$ relative to $\varepsilon(O_8)$ is only 9 meV/atom – much smaller than the 0 K value of 60.8 meV/atom. The larger entropy of $\eta'$ is now sufficient to compensate for this smaller correction and $\eta'$ is thus the preferred phase at high $T$ (Fig. 6). We have recomputed the Gibbs free energies of the two structures as a function of $T$ by interpolating the HSE06 correction between the 0 and 1200 K values. The final result is that at 50 GPa $\eta'$-$O_2$ becomes thermodynamically stable at temperatures above about 780 K.

Note that the 0 K enthalpy differences between the two structure decrease as a function of $P$. The transition temperature between them is therefore projected to decrease with pressure. Our estimate for the Clapeyron slope ($dT/dP$) of the $\varepsilon(O_8)$–$\eta'(O_2)$ phase line is -6.86 K/GPa (GGA) and -6.01 K/GPa (HSE06) at 50 GPa and 780 K. Indeed, the $\eta'$ structure becomes competitive at low temperature for pressures above 115 GPa [20]; stability analysis for this pressure region will be presented in a separate report.

## Conclusions

We have determined that the experimentally proposed $\eta'$ structure is mechanically unstable at low $T$ within a classical ion dynamics treatment due to soft phonon modes. However, it is stabilized at finite $T$, where the thermally renormalized phonons also contribute to it having a relatively large entropy. In the presence of thermal disorder, the differences between the local structural order and electronic properties of $\varepsilon(O_8)$ and $\eta'$ diminish. The interplay of all these factors - anharmonicity, exchange effects, and thermal disorder, results in the metallic $\eta'$ becoming the thermodynamically stable phase at elevated $T$. At 50 GPa, we predict the transition to take place at around 780 K.

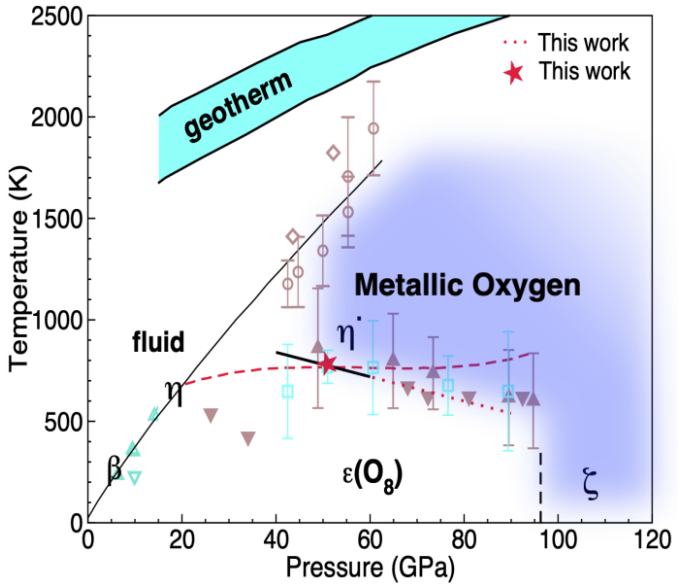


**Fig. 7** Phase diagram of oxygen comparing the $\varepsilon$-$\eta'$ transition computed in this work with previous experimental data taken from Ref.[38]. The computed transition at 50 GPa is shown with a red star, and the computed Clapeyron slope at that $P$-$T$ point as a short solid black line. The dotted red line is an extrapolation of the Clapeyron slope. Open triangles up and down are melting and $\varepsilon$-$\beta$ transition, respectively. Black filled triangles down represent conditions where the $\varepsilon$-$O_2$ is stable. Open squares and filled triangles up with error bars are $\varepsilon$-$\eta'$ transition determined by x-ray and Raman, respectively. The curved dashed line is the proposed $\varepsilon$-$\eta'$ transition. Open circles with the error bars represent the melting points. Green diamond points represent the melting points from ref.[46]. The dashed vertical line represents where the metallization takes place in solid oxygen. The red solid line is the melting line calculated from the Simon equation as described in ref.[38].The Earth's geotherm region is taken from ref.[47].

The $\varepsilon(O_8)$ to $\eta'$ phase boundary has negative slope. At 50 GPa, $dT/dP = -6.01$ K/GPa within HSE06 or $-6.86$ K/GPa within GGA-PBE. The computed $\varepsilon(O_8)$-$\eta'$ phase transition at 50 GPa, and an estimate for its phase boundary as a function of pressure (an extrapolation from the Clapeyron slope) are shown in Fig. 7 together with experimental data for the oxygen phase transitions. Our results suggest that at pressures above $\sim 100$ GPa $\eta'$ is energetically competitive even at room temperature. However, we caution that a few meV/atom is within the accuracy of first principles calculations. When energy differences between competing structures are this small, it is not possible to make a definitive conclusion for the thermodynamic stability structure based on the calculations alone. We expect that this report will stimulate further theoretical and experimental studies of the high pressure and/or temperature phase diagram of oxygen.

## Computational Methods

First principles density-functional theory (DFT) [48] and hybrid exchange calculations were performed with the ABINIT[49] and VASP[50,51] packages. All comparisons of relative energies between structures were determined from calculations using the same code and identical simulation parameters.

### Density-functional theory calculations

Structural optimizations and enthalpy calculations within the generalized gradient approximation (GGA) [51,52] and the local density approximation (LDA)[53] were performed with ABINIT using Troullier-Martins Pseudopotentials[54], a plane-wave expansion with a 80-Hartree cut-off, and $\mathbf{k}$-point grids of $16^3$, $4^3$, and $12\times12\times10$ for $\eta'$, $\varepsilon$ $(O_8)$, and $\zeta$ $(C2/m)$ phases, respectively, ensuring enthalpy convergence to better than 1 meV/atom. Structure symmetry analysis was performed using the FINDSYM code[55] with tolerance 0.001 at all pressure points in order to identify the symmetry of the optimized structures.

Phonon calculations using Density-Functional Perturbation Theory (DFPT)[56] as employed in ABINIT[49] were carried out with the same convergence parameters used to calculate the enthalpies of the corresponding structures. For the $\varepsilon(O_8)$ phase, a $4^3$ $\mathbf{q}$-point phonon grid for computing the dynamical matrices was sufficient to achieve convergence for Helmholtz free energies and entropy better than 1 meV/atom. For $\eta'$, the dynamical matrices were computed on $3^2\times5$ , $3^2\times9$, $5^3$, and $7^2\times5$ $\mathbf{q}$-point grids, in all cases yielding imaginary phonon frequencies.

First principle molecular dynamic (FPMD) simulations were carried out using finite-$T$ DFT[48] within PBE-GGA[51,52,57] and VASP[50,51]. The simulations were with 300-atom supercells, the $\Gamma$ $\mathbf{k}$-point, a 6-electron projector augmented wave pseudopotential, and a 1000 eV plane-wave cut-off in the canonical $NVT$ (constant number of particles, $N$, volume $V$, and $T$) ensemble using Born-Oppenheimer dynamics with a Nos*é*-Hoover thermostat. For each $V$ and $T$, the system was initially equilibrated for 2 ps and then run additional 6 ps or more using a 0.75 fs ionic time step to adequately sample and extract equilibrium statistical properties.

### Hybrid exchange calculations

Hybrid exchange calculations within the Heyd-Scuseria-Ernzerhof approximation (HSE06) [42] were carried out with VASP. We have used the standard mixture of 25% of Hartree-Fock exact exchange and 75% of the PBE exchange for short-range interactions, and PBE only exchange for the long-range interactions. The range separation is at around 4 Å.

Full structural optimizations within HSE06 were performed using a 1000 eV plane-wave cut-off and slightly reduced $\mathbf{k}$-point grids: $(12\times12\times4)$ for $\eta'$ and $(6\times6\times6)$ for $\zeta(C2/m)$, ensuring convergence of relative enthalpies to better than 2 meV/atom. Additionally, HSE06 electronic band structures were calculated on both HSE06 and GGA relaxed structures.

To evaluate the HSE06 corrections at finite temperature, we have performed HSE06 calculations on atomic configurations taken from the FPMD trajectories at 1200 K. For each structure, 5-10 equally spaced (in time) configurations were taken from the trajectories and their energies computed within GGA-PBE and HSE06 with exactly the same simulation parameters. ($\Gamma$ k-point and 1000 eV plane wave cut off). We verified that the fluctuations in the energy differences between HSE06 and GGA-PBE are negligible, which indicates that the GGA-PBE ensemble is sufficient for this analysis.

### Gibbs free energies

Gibbs free energies ($G$) at finite $T$ were computed as $G = E_0 + P_0V + P_{\rm ph}V + U_{\rm ph} - TS$, where $E_0$ and $P_0$ are the 0 K DFT energy and pressure, $U_{\rm ph}$ and $P_{\rm ph} = -\frac{\partial F_{\rm ph}}{\partial V}|_{N,T}$ are the phonon internal energy and pressure, $S$ is the entropy, and $F_{\rm ph} = U_{\rm ph} - TS$. Here $U_{\rm ph}$ and $S$ are obtained by integrating vibration density of states (VDOS), which for $\eta'$ are calculated by taking Fourier transforms of velocity autocorrelation functions (VACF). Although $S$ is calculated using a harmonic partition function, the VDOS from PFMD represent thermally renormalizes phonons and capture most of the anharmonic free energy[45]. For $\varepsilon(O_8)$, VDOS are calculated from DFPT. We confirmed that the harmonic approximation for $\varepsilon(O_8)$ is sufficient by comparing the DFPT with VDOS from FPMD at $\sim$ 50 GPa at 1200 K.

## Acknowledgments

We thank Prof. R. Hoffmann and Dr. V. Askarpour for helpful discussions. This work was supported by NSERC, Acenet and LLNL. S.A.B. performed work at LLNL under the auspices of the US Department of Energy under contract No. DE-AC52-07NA27344.

**Data availability statements:**
All data generated or analyzed during this study are included in this published article (and its supplementary information files).
**Author contributions statement:**
S.A.B designed the research, S.F.E performed the research, S.F.E. and S.A.B. analyzed the data and wrote the paper.
**Competing Interests:**
There are no conflicts to declare.

## Notes and references

1 Y. Freiman, H. Jodl and Y. Crespo, *Physics Reports*, 2018, **743**, 1 – 55.
2 Y. Akahama, H. Kawamura, D. Häusermann, M. Hanfland and O. Shimomura, *Phys. Rev. Lett.*, 1995, **74**, 4690–4693.
3 Y. Freiman and H. Jodl, *Physics Reports*, 2004, **401**, 1–228.
4 L. F. Lundegaard, G. Weck, M. I. McMahon, S. Desgreniers and P. Loubeyre, *Nature*, 2006, **443**, 201–204.
5 E. M. Hörl, *Acta Crystallographica*, 1962, **15**, 845–850.
6 R. LeSar and R. D. Etters, *Phys. Rev. B*, 1988, **37**, 5364–5370.
7 L. F. Lundegaard, C. Guillaume, M. I. McMahon, E. Gregoryanz and M. Merlini, *The Journal of Chemical Physics*, 2009, **130**, 164516.
8 R. J. Meier and R. B. Helmholdt, *Phys. Rev. B*, 1984, **29**, 1387–1393.
9 D. Schiferl, D. T. Cromer, L. A. Schwalbe and R. L. Mills, *Acta Crystallographica Section B*, 1983, **39**, 153–157.
10 F. A. Gorelli, M. Santoro, L. Ulivi and M. Hanfland, *Phys. Rev. B*, 2002, **65**, 172106.
11 I. N. Goncharenko, O. L. Makarova and L. Ulivi, *Phys. Rev. Lett.*, 2004, **93**, 055502.
12 S. Desgreniers, Y. K. Vohra and A. L. Ruoff, *The Journal of Physical Chemistry*, 1990, **94**, 1117–1122.
13 K. Shimizu, K. Suhara, M. Ikumo, M. I. Eremets and K. Amaya, *Nature*, 1998, **393**, 767–769.
14 L. Zhu, Z. Wang, Y. Wang, G. Zou, H.-k. Mao and Y. Ma, *Proceedings of the National Academy of Sciences*, 2012, **109**, 751–753.
15 T. Nomura, Y. H. Matsuda, S. Takeyama, A. Matsuo, K. Kindo, J. L. Her and T. C. Kobayashi, *Phys. Rev. Lett.*, 2014, **112**, 247201.
16 B. Militzer, F. m. c. Gygi and G. Galli, *Phys. Rev. Lett.*, 2003, **91**, 265503.
17 S. Serra, G. Chiarotti, S. Scandolo and E. Tosatti, *Phys. Rev. Lett.*, 1998, **80**, 5160–5163.
18 R. Gebauer, S. Serra, G. L. Chiarotti, S. Scandolo, S. Baroni and E. Tosatti, *Phys. Rev. B*, 2000, **61**, 6145–6149.
19 J. B. Neaton and N. W. Ashcroft, *Phys. Rev. Lett.*, 2002, **88**, 205503.
20 S. Elatresh, *PhD thesis*, Dalhousie University, 2015.
21 S. Elatresh and S. Bonev, APS Shock Compression of Condensed Matter Meeting Abstracts, 2013, p. B3.005.
22 L. T. Anh, M. Wada, H. Fukui, T. Kawatsu and T. Iitaka, *Scientific Reports*, 2019, **9**, 8731.
23 A. J. Ochoa-Calle, C. M. Zicovich-Wilson, R. Hernández-Lamoneda and A. Ramírez-Solís, *Journal of Chemical Theory and Computation*, 2015, **11**, 1195–1205.
24 A. J. Ochoa-Calle, C. M. Zicovich-Wilson and A. Ramírez-Solís, *Phys. Rev. B*, 2015, **92**, 085148.
25 A. Ochoa-Calle, C. Zicovich-Wilson and A. Ramírez-Solís, *Chemical Physics Letters*, 2015, **638**, 82 – 86.
26 A. Ramirez-Solis, C. M. Zicovich-Wilson, R. Hernandez-Lamoneda and A. J. Ochoa-Calle, *PCCP*, 2017, **19**, 2826–2833.
27 S. W. Johnson, M. Nicol and D. Schiferl, *Journal of Applied Crystallography*, 1993, **26**, 320–326.
28 G. Weck, P. Loubeyre and R. LeToullec, *Phys. Rev. Lett.*, 2002, **88**, 035504.
29 H. Fukui, L. T. Anh, M. Wada, N. Hiraoka, T. Iitaka, N. Hirao, Y. Akahama and T. Irifune, *Proceedings of the National Academy of Sciences*, 2019, **116**, 21385–21391.
30 Y. Akahama and H. Kawamura, *Phys. Rev. B*, 1996, **54**, R15602–R15605.
31 F. A. Gorelli, L. Ulivi, M. Santoro and R. Bini, *Phys. Rev. Lett.*, 1999, **83**, 4093–4096.
32 Y. Akahama and H. Kawamura, *Phys. Rev. B*, 2000, **61**, 8801–8805.
33 S. F. Agnew, B. I. Swanson and L. H. Jones, *The Journal of Chemical Physics*, 1987, **86**, 5239–5245.
34 Y. Akahama, H. Fujihisa, N. Hirao and Y. Ohishi, *Japanese J. App. Phys.*, 2019, **58**, 095502.
35 G. Weck, S. Desgreniers, P. Loubeyre and M. Mezouar, *Phys. Rev. Lett.*, 2009, **102**, 255503.
36 H. Fujihisa, Y. Akahama, H. Kawamura, Y. Ohishi, O. Shimomura, H. Yamawaki, M. Sakashita, Y. Gotoh, S. Takeya and K. Honda, *Phys. Rev. Lett.*, 2006, **97**, 085503.
37 Y. Meng, P. J. Eng, J. S. Tse, D. M. Shaw, M. Y. Hu, J. Shu, S. A. Gramsch, C.-c. Kao, R. J. Hemley and H.-k. Mao, *Proceedings of the National Academy of Sciences*, 2008, **105**, 11640–11644.
38 A. F. Goncharov, N. Subramanian, T. R. Ravindran, M. Somayazulu, V. B. Prakapenka and R. J. Hemley, *The Journal of Chemical Physics*, 2011, **135**, 084512.
39 M. Santoro, E. Gregoryanz, H.-k. Mao and R. J. Hemley, *Phys. Rev. Lett.*, 2004, **93**, 265701.
40 I. N. Goncharenko, *Phys. Rev. Lett.*, 2005, **94**, 205701.
41 Y. Ma, A. R. Oganov and C. W. Glass, *Phys. Rev. B*, 2007, **76**, 064101.
42 J. Heyd, G. E. Scuseria and M. Ernzerhof, *The Journal of Chemical Physics*, 2006, **124**, 219906.
43 B. Boates and S. A. Bonev, *Phys. Rev. Lett.*, 2013, **110**, 135504.
44 A. M. Teweldeberhan, J. L. DuBois and S. A. Bonev, *Phys. Rev. B*, 2012, **86**, 064104.
45 A. M. Teweldeberhan, J. L. Dubois and S. A. Bonev, *Phys. Rev. Lett.*, 2010, **105**, 235503.
46 L. R. Benedetti, D. Antonangeli, D. L. Farber and M. Mezouar, *Applied Physics Letters*, 2008, **92**, 141903.
47 M. Isshiki, T. Irifune, K. Hirose, S. Ono, Y. Ohishi, T. Watanuki, E. Nishibori, M. Takata and M. Sakata, *Nature*, 2004, **427**, 60–63.
48 W. Kohn and L. J. Sham, *Phys. Rev.*, 1965, **140**, A1133–A1138.
49 X. Gonze, B. Amadon, P.-M. Anglade, J.-M. Beuken, F. Bottin, P. Boulanger, F. Bruneval, D. Caliste, R. Caracas, M. Cote, T. Deutsch, L. Genovese, P. Ghosez, M. Giantomassi, S. Goedecker, D. Hamann, P. Hermet, F. Jollet, G. Jomard, S. Leroux, M. Mancini, S. Mazevet, M. Oliveira, G. Onida, Y. Pouillon, T. Rangel, G.-M. Rignanese, D. Sangalli, R. Shaltaf, M. Torrent, M. Verstraete, G. Zerah and J. Zwanziger, *Computer Physics Communications*, 2009, **180**, 2582 – 2615.
50 G. Kresse and J. Hafner, *Phys. Rev. B*, 1993, **47**, 558–561.
51 G. Kresse and J. Furthmüller, *Phys. Rev. B*, 1996, **54**, 11169–11186.
52 J. P. Perdew, K. Burke and M. Ernzerhof, *Phys. Rev. Lett.*, 1996, **77**, 3865–3868.
53 J. P. Perdew and A. Zunger, *Phys. Rev. B*, 1981, **23**, 5048–5079.
54 N. Troullier and J. L. Martins, *Phys. Rev. B*, 1991, **43**, 1993–2006.
55 H. T. Stokes and D. M. Hatch, *Journal of Applied Crystallography*, 2005, **38**, 237–238.
56 X. Gonze, *Phys. Rev. B*, 1997, **55**, 10337–10354.
57 J. P. Perdew, K. Burke and M. Ernzerhof, *Phys. Rev. Lett.*, 1997, **78**, 1396–1396.